RSC Advances

PAPER

View Article Online
View Journal | View Issue

Cite this: *RSC Adv.*, 2026, **16**, 19300

Investigation of positron scattering from atomic fluorine and fluorine-containing molecules

Ashutosh Yadav and Bobby Antony *

We report positron scattering cross sections of fluorine and fluorine-containing molecules across an energy range from 1 to 5000 eV. Targets considered in the present study are F, F_2, HF, CF_4, C_2F_6, C_6F_6, CHF_3, $C_2H_3F_3$, and $C_2H_2F_2$. Elastic, inelastic, total, and positronium formation cross sections were calculated using the optical potential approach, and the ionisation cross sections are estimated employing the complex scattering potential-ionisation contribution method. The computed results are in satisfactory agreement with available theoretical data. Comparison with experiments shows excellent agreement in the high-energy range; however, discrepancies are observed at lower energies, attributed to deficiencies in the polarisation potential model used and, in part, to the difficulty in resolving forward-angle scattering effects in experimental measurements. Positron interactions with these molecules are important in plasma, astrophysics, and radiation physics, where ionisation, energy losses, and the formation and destruction of positronium are significant. The positron scattering cross-sections are primary inputs for modelling in astrophysics, materials science, and medical imaging, such as positron emission tomography.

Received 16th February 2026
Accepted 21st March 2026

DOI: 10.1039/d6ra01378c

rsc.li/rsc-advances

1 Introduction

The interaction of the positron, the antiparticle of the electron, with molecules is appealing due to its unique properties. Positron collisions exhibit distinct characteristics compared to electron collisions, primarily due to the absence of exchange interaction with the target electrons, and positrons experience a repulsive interaction with nuclei and an attractive interaction with the electron clouds of atoms.[1] Additionally, there exists a very short-lived bound state of electron and positron known as positronium, which is a prominent inelastic channel during positron collisions with atoms and molecules. Positronium annihilates by producing two extremely energetic gamma photons,[2] which can penetrate materials deeply and have applications in surface and interface analysis, defect characterisation *via* positron annihilation spectroscopy (PAS), and detecting defects using annihilation spectra models.[3] Cross-section data, such as ionisation, electronic excitation, and positronium formation, help understand various phenomena in interstellar gases.[4,5] For example, how rapidly positrons lose energy, identify astrophysical positron sources,[6] and to determine the reaction rate.[7] Positron emission tomography (PET) is a medical imaging technique that utilises the positron cross-section to image the metabolism or function of the tissue in three dimensions. Fluorodeoxyglucose, a positron-emitting fluorine isotope, is used in PET.[8–10]

The availability of high-resolution steady positron beams has facilitated high-quality experimental research in positron collision physics in the last couple of decades. Unfortunately, the number of active research groups in positron scattering studies has dwindled, including those focused on theory. Most experimentalists use a Penning trap, which combines magnetic and electric fields to confine positrons. A special Penning trap, which is a buffer-gas trap, utilises carbon tetrafluoride, where positrons are accumulated through inelastic collisions with gas molecules. Buffer-gas traps are used for positron beams to perform scattering experiments,[11] particularly in areas such as materials science, dense positronium states, and anti-hydrogen formation.[12] Theoretical methodologies such as convergent close-coupling,[13] the Swinger multichannel method,[14] and the optical potential method predict positron scattering cross-sections for various applications.[10,15,16]

In the present study, we analyse the positron scattering from F, HF, F_2, CHF_3, CF_4, $C_2H_3F_3$, C_2F_6, $C_2H_2F_2$ and C_6F_6 molecules. Several electron scattering cross sections are available[17–19] for these targets; however, positron studies are limited, despite being crucial to many applied areas. For polyatomic hydrocarbons that contain fluorine, only the total cross section is available. However, the inelastic cross-sections (*e.g.* ionisation, positronium formation, and excitation) are quite relevant, especially for astrochemistry and plasma physics. Previous results are available for F, HF, F_2, CHF_3, CF_4, C_2F_6 and C_6F_6 by Mori *et al.*,[20] who reported theoretical cross sections in the energy range of 0.01 to 5000 eV using the single-centre convergent close-coupling method. Baluja and Jain calculated the total

Department of Physics, Indian Institute of Technology (ISM) Dhanbad, JH 826004, India. E-mail: bobby@iitism.ac.in

cross section for CF_4 in the energy range 10 to 5000 eV using the spherical complex optical potential method.[21] Recently, they also calculated total, ionisation and elastic cross section with forward angle correction for $C_2H_2F_2$ (ref. 22) in the energy range of 0.1 to 4000 eV. Experimental total cross sections for CHF_3, CF_4, $C_2H_3F_3$, and C_2F_6 are reported for the energy range 0.6 to 600 eV by Sueoka *et al.*[23–25] and for C_6F_6 and $C_2H_2F_2$ by Makochekanwa *et al.*[19,26] in the energy range of 0.4 to 1000 eV using a retarding potential time-of-flight method.

The cross-section data for these targets are crucial to many applications. For instance, the reliable positron scattering cross section of fluorine is important, as it is used to estimate the cross section of complex molecules having a fluorine atom employing the independent atom model. On the other hand, it is challenging to measure the cross-section for the F_2 experimentally as it is highly reactive with metals. HF was recently discovered in the interstellar medium,[27] and hence the positron scattering study from this molecule will be of great significance for the understanding of its astrochemistry.[28] Perfluorocarbons (CF_4, C_2F_6, C_6F_6) are used in plasma etching owing to their chemistry, naturally giving high etch rates, good selectivity and anisotropy. Also, CF_4 positron collision cross-sections are widely employed for positron cooling and buffer gas traps,[29,30] due to their high inelastic cross-sections. C_2F_6 are used to etch SiO_2 and related materials. Hydrofluorocarbon (CHF_3, $C_2H_3F_3$, $C_2H_2F_2$) molecules are intermediates of pure hydrocarbon and pure perfluorocarbon. They are used in reactive ion etching as replacements for perfluorocarbons, as they are "super" greenhouse gases and provide better selectivity.[31,32] These gases are found in the environment. Perfluorocarbons are high global warming potential (GWP) gases.[33] The present positron scattering study will help in understanding their radiation chemistry.

Several interaction processes occur between target molecules and positrons; therefore, accurate cross-section data are required to understand and model these interactions for biological, interstellar, and plasma chemistry. Cross sections serve as essential input parameters in theoretical and computational modeling. It also needs the transport data, mean free path, drift velocity, and mean energy, which can be obtained from the cross sections.[34] The present target cross-section reported here has inadequate data. So a comprehensive data set for elastic (Q_{el}), inelastic (Q_{inel}), total (Q_{total}), ionisation (Q_{ion}) and positronium formation (Q_{ps}) cross sections in the energy range 1–5000 eV is reported using the quantum mechanical optical potential approach.

2 Theoretical methodology

The spherical complex optical potential (SCOP) and complex scattering potential ionisation contribution (CSP-ic) methods are utilised for the calculation of positron scattering cross sections over an energy range from 1 eV to 5 keV, ensuring broad coverage of both low- and high-energy regimes. This method has proven to provide reliable electron and positron integral elastic and inelastic cross sections for atoms and molecules. The method can also predict elastic differential and momentum transfer cross sections as well.[4,10,16,35–39]

The optical potential approach is based on the principle of optics, where a ray of light is scattered elastically (refraction) and inelastically (absorption). In the case of the scattering of positrons from a target, the interaction potential is represented as a complex potential, as both elastic and inelastic collisions occur during the interaction. The real part of the potential stands for the elastic collisions due to static (V_{st}) and polarisation (V_{pol}) potentials. The imaginary part corresponds to the inelastic collisions depicted by the absorption potential (V_{abs}) representing the loss of energy during the interaction. The interaction between the incident positron and the target is thus modelled by a complex optical potential given by:

$$V_{opt} = V_{st} + V_{pol} + iV_{abs} \quad (1)$$

where V_{st} stands for the Coulomb interaction with the unperturbed target charge cloud. This is constructed using the charge density derived from Hartree–Fock atomic wavefunctions[40] expanded from the centre of the molecule or group and then renormalised to account for the total number of target electrons. V_{pol} represents the distortion of the target's electron cloud due to the incoming positron's electric field. We use the model by Zhang *et al.*,[41] which incorporates short-range correlation as well as long-range polarisation by using the Perdew and Zunger[42] model potential. V_{abs} models the loss of flux due to inelastic processes, such as ionisation, excitation, and positronium formation. Here we have adopted the model of Reid and Wadehra.[43]

In the Reid and Wadehra[43] model, the threshold of absorption $\Delta(E)$ is considered to be the first excited state (E_i). However, the positronium formation threshold, Δ_p, is usually lower than the E_i; hence, positronium formation is neglected in the calculation, underestimating the inelastic part. To account for the channels with thresholds below E_i (*e.g.*, positronium formation), changes are made in the inelastic threshold $\Delta(E)$ by adopting the method proposed by Chiari *et al.*[44] That is,

$$\Delta(E) = \mathrm{IP} - (\mathrm{IP} - \Delta_p)\exp\left(-\frac{E_i - \Delta_p}{E_m}\right) \quad (2)$$

Here Δ_p is the positronium formation threshold, E_i the incident positron energy, IP the ionisation potential, and E_m the energy at which the inelastic cross section reaches a maximum.

The Schrödinger equation with this complex optical potential is solved by partial wave analysis using the Numerov method to obtain complex phase shifts, δ_l. From these, the elastic (Q_{el}) and inelastic cross sections (Q_{inel}) are computed as:

$$Q_{el} = \frac{\pi}{k^2}\sum_{l=0}^{\infty}(2l+1)\left|\eta_l e^{2i\mathrm{Re}\delta_l} - 1\right|^2, \quad (3)$$

$$Q_{inel} = \frac{\pi}{k^2}\sum_{l=0}^{\infty}(2l+1)\left(1-\eta_l{}^2\right), \quad (4)$$

$\eta_1 = e^{-2\mathrm{Im}\delta_l}$, which is the inelasticity factor. To estimate the positronium formation cross section, the modified total

inelastic cross section (Q_{inel}) with Ps (using threshold, $\Delta(E)$, as in eqn (2)) and unmodified inelastic cross (Q_{in}) without Ps are calculated by SCOP. Then, the difference between these two inelastic cross sections gives the positronium formation (Q_{Ps}) cross section. To separate the entire inelastic cross section into individual contributions from direct ionisation (Q_{ion}), positronium formation (Q_{Ps}), and electronic excitation (Q_{exc}), we use the CSP-ic method. This involves defining:

$$Q_{in} = Q_{inel} - Q_{ps} = Q_{ion} + Q_{exc} \quad (5)$$

A ratio function $R(E_i) = \frac{Q_{ion}}{Q_{in}}$ is defined to calculate Q_{ion} from Q_{in} which is given as

$$R(E_i) = 1 - C_1\left[\frac{C_2}{U+a} + \frac{\ln(U)}{U}\right] \quad (6)$$

where C_1, C_2, and a are unknown and obtained using boundary conditions and target properties. For further details, refer to the papers published earlier.[4,10,45,46] Once we have this ratio, we can estimate Q_{ion}, the direct ionisation cross section from the Q_{in} using the relation:

$$Q_{ion} = R(E_i) \times Q_{in} \quad (7)$$

and the total ionisation cross section is:

$$Q_{ion,total} = Q_{ion} + Q_{ps} \quad (8)$$

CSP-ic is a semi-empirical method that provides a reliable estimate of the ionisation cross-section with an uncertainty of ± 7%[47] at the peak of the inelastic cross-section and near zero at low and high energies. The present study involves a set of large molecules. Hence, we have used modified additivity rule (MAR) to handle multicentred systems in which the molecules are divided into multiple groups based on the bond length and atomic radius. For present targets HF, CH, CH_2, and CH_3 form single groups within CHF_3, $C_2H_2F_2$, and $C_2H_3F_3$ targets. Further, in MAR, the cross section of each group is calculated using the molecular properties like ionization potential, bond length, and polarizability of the molecule.[47,48] Then these individual cross sections are added to get the total cross section for the molecules. This method as also named as group additivity rule. SCE method is used to calculate the charge density of the group in which the charge density of lighter hydrogen atom is expanded at the center of the heavier atoms (C and F).[49] The charge density is used to calculate interaction potentials of the target molecules. The properties such as bond length, ionisation potential, and polarisability incorporated in the positron scattering cross-section calculation are taken from the CCCBDB,[50] which are listed in Table 1.

Table 1 Target properties

Target	IP (eV)	Δ_p (eV)	α (Å^3)
F	17.420	10.620	0.557
F_2	15.697	8.897	1.160
HF	16.030	9.230	0.800
CF_4	14.700	7.900	2.824
C_2F_6	13.600	6.800	4.668
C_6F_6	9.800	3.000	9.580
CHF_3	13.860	7.060	2.801
$C_2H_2F_2$	10.290	3.490	4.203
$C_2H_3F_3$	13.260	6.460	4.400

3 Results and discussion

Positron scattering cross sections, Q_{el}, Q_{inel}, Q_{total}, Q_{ps} and Q_{ion} for the target atom and molecules are presented in this section and compared with available experimental results of Sueoka *et al.*,[23–25] Makochekanwa *et al.*[19,26] and theoretical results of Mori *et al.*[20] and Baluja *et al.*[21,22]

3.1 Cross sections of target molecules

Fluorine is one of the most reactive elements in the periodic table, and it exists in nature in diatomic form. Hence, no measurements on positron interaction are available. The only available cross sections are by Mori *et al.*[20] who performed calculations for the same. Fig. 1a presents the total and elastic cross-section of the F atom in the energy range of 1 eV to 5000 eV. Below 10 eV, the elastic cross section merges with the total cross section as the inelastic channels are initially absent. However, with the opening of inelastic channels, the total cross section starts to increase rapidly, reaching a maximum of 3.464 Å^2 at about 40 eV. Then, it falls with energy and reaches a minimum of 0.227 Å^2 at 5000 eV. The Q_{el}, on the other hand, starts decreasing from 8 eV onwards, where the cross section is 1.637 Å^2, and falls monotonously to 0.102 Å^2 at 5000 eV. The present Q_{total}, Q_{el} are compared with the results of Mori *et al.*[20] Qualitatively, our results agree with the shape of the cross-section, but quantitatively, there is a gap between the two. The present cross section is high between 1 eV and 200 eV, while above 200 eV, Mori *et al.*'s[20] cross section overestimates for both Q_{total} and Q_{el}. The difference observed here is primarily due to the methodology involved in the calculation. We have used the SCOP method, in which Schrödinger equation is solved using model potentials[40,41] to obtain the phase shift, from which we calculate the cross sections. While Mori *et al.*[20] have used single-centre convergent close-coupling calculations to obtain the T-matrix elements from which cross sections are derived. However, at high energies, they come quite close to each other.

Fig. 1b presents the inelastic, ionisation, and positronium formation cross-sections for the fluorine atom. The positronium formation channel opens at 10.62 eV and contributes the maximum to the inelastic channel in the 10–100 eV range. The Q_{ps} peaks are at about 25 eV, where the cross section is 1.299 Å^2 and decreases to 0.037 Å^2 at 200 eV. It becomes zero at energies beyond 500 eV. The present Q_{ps} is compared with the available result of Mori *et al.*[20] The present result is higher than theirs with a peak at the same energy. However, the shapes of both curves are quite consistent with each other. The ionisation channel opens above 17.42 eV, with the present cross section showing reasonable agreement with the data of Mori *et al.*[20] over the entire energy range, except for the shift in peak position.

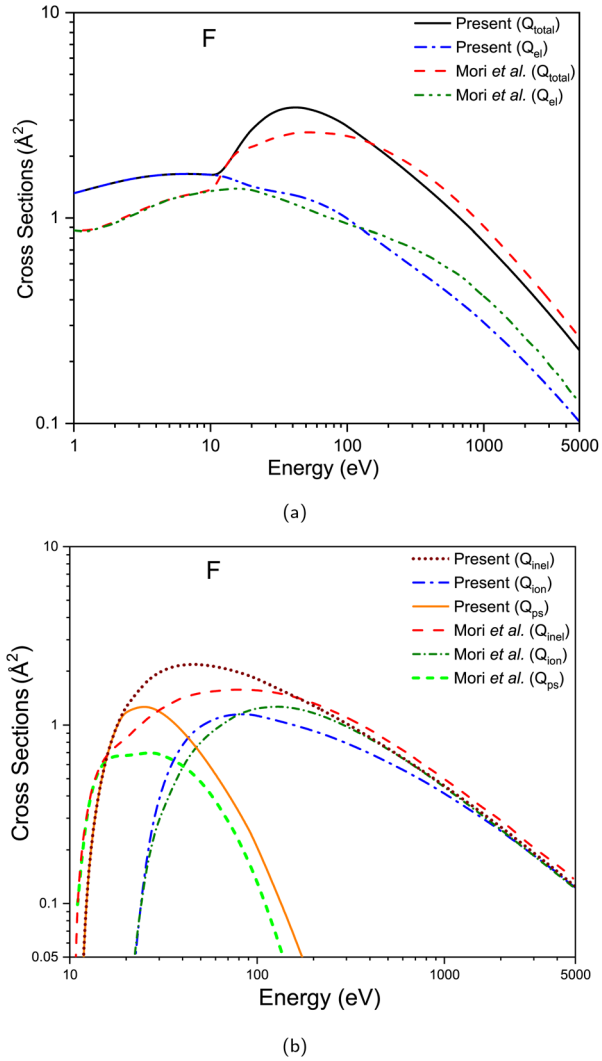

Fig. 1 Positron scattering from fluorine (a) Q_{total}: present – black solid, Mori*et al.* – red dash; Q_{el}: present – blue dash dot, Mori *et al.* – olive dash dot dot. (b) Q_{inel}: present – wine short dot, Mori *et al.* – red dash; Q_{ps}: present – orange solid, Mori *et al.* – green short dash; Q_{ion}: present – blue dash dot, Mori *et al.* – olive short dash dot.

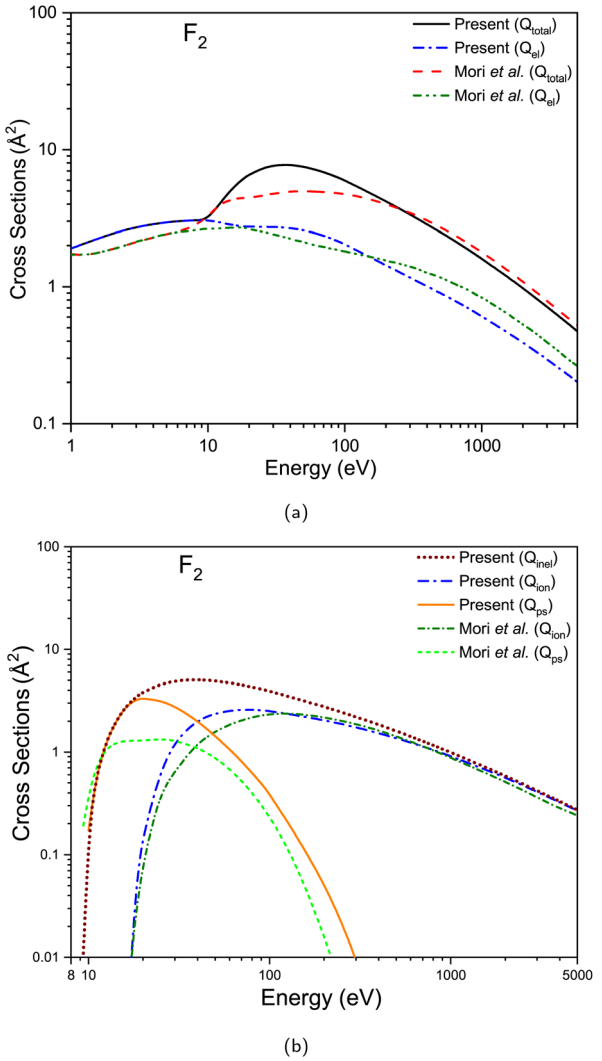

Fig. 2 Positron scattering from a F_2 (a) Q_{total}: present – black solid, Mori *et al.* – red dash; Q_{el}: present – blue dash dot, Mori *et al.* – olive dash dot dot. (b) Q_{inel}: present – wine short dot, Mori *et al.* – red dash; Q_{ps}: present – orange solid, Mori *et al.* – green short dash; Q_{ion}: present – blue dash dot, Mori *et al.* – olive short dash dot.

The peak of the present Q_{ion} is 1.15 Å^2 at 80 eV, while that of Mori *et al.*[20] is shifted towards the left, with slightly lower magnitude. The present Q_{inel}, which includes Q_{ps} and Q_{exc}, starts at 9 eV, peaks at 45 eV, then merges gradually with Q_{ion} as expected. The present Q_{inel} is also compared with that of Mori *et al.*[20] The shape and magnitude compare similarly to each other Q_{ion} and are in good agreement. Overall, both Q_{ion} and Q_{inel} agrees reasonably well with that of Mori *et al.*[20]

Fig. 2 presents the integral cross-sections for the F_2 molecule and compares them with the available results from Mori *et al.*[20] The elastic and total cross-sections are presented in Fig. 2a from 1 eV onwards. The Q_{total} increases gradually to 3.046 Å^2 at 9 eV, then dips a little, and thereafter enhances sharply to 7.758 Å^2 at 35 eV. The hump-like structure observed around 30–50 eV is due to the positronium formation channel, which has a significant probability in this energy region, as seen in Fig. 2b. Beyond that, the cross section decreases with energy, and at 5000 eV, it reaches as low as 0.472 Å^2. It is in good agreement with Mori *et al.*[20] above 200 eV; below that, the present results are higher, except around 10 eV. The reason for this deviation is similar to what we have seen for Fig. 1. However, both Q_{el}, the present one and that of Mori *et al.*,[20] match reasonably well throughout the energy range.

Fig. 2b presents the positronium formation, ionisation and total inelastic cross sections. The present Q_{ps} data are in good agreement with Mori *et al.*[20] till around 20 eV. Above that, the present values are quite higher compared to Mori *et al.*[20] However, the overall shapes are consistent with each other, with the peak at the same energy and looking similar to that of the atomic fluorine. Both Q_{ion} are in good agreement throughout the energy range, with their peak at 80 eV, the same as that of Mori *et al.*,[20] with a slight difference in magnitude. The inelastic

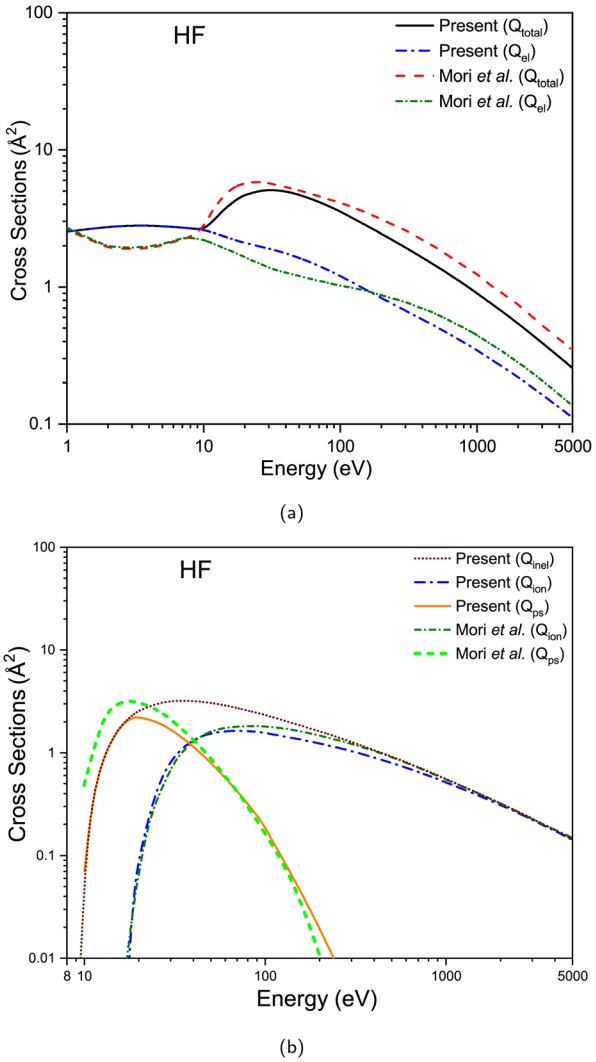

Fig. 3 Positron scattering from a HF (a) Q_{total}: present – black solid, Mori *et al.* – red dash; Q_{el}: present – blue dash dot, Mori *et al.* – olive dash dot dot. (b) Q_{inel}: present – wine short dot, Mori *et al.* – red dash; Q_{ps}: present – orange solid, Mori *et al.* – green short dash; Q_{ion}: present – blue dash dot, Mori *et al.* – olive short dash dot.

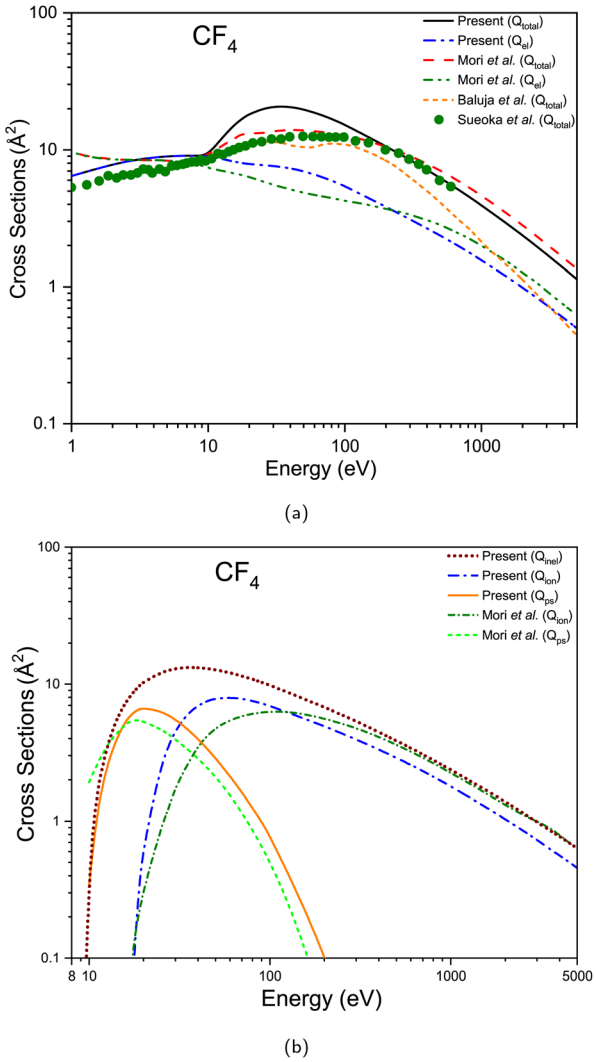

Fig. 4 Positron scattering from CF_4 (a) Q_{total}: present – black solid, Mori *et al.* – red dash, Baluja *et al.* – orange short dash, Sueoka *et al.* – olive solid circle; Q_{el}: present – blue dash dot, Mori *et al.* – olive dash dot dot. (b) Q_{inel}: present – wine short dot; Q_{ps}: present – orange solid, Mori *et al.* – green short dash; Q_{ion}: present – blue dash dot, Mori *et al.* – olive short dash dot.

cross section, which starts from 0.002 Å^2 at 9 eV, peaks around 40 eV with 5.06 Å^2 and then lowers to 0.272 Å^2 at 5000 eV. Qualitatively, the overall comparison with the results of Mori *et al.*[20] looks good.

In Fig. 3, elastic and inelastic cross sections are presented for the HF molecule. Unlike previous cases, the cross section reported by Mori *et al.*[20] agrees reasonably well with the present results.

The elastic and total cross section starts at a high magnitude of 2.524 Å^2 at 1 eV, as shown in Fig. 3a. The cross section is almost constant till around 11 eV and then increases to reach a maximum of 5.091 Å^2 at energy 30 eV. Following that, it begins to decline to a value of 0.255 Å^2 at 5000 eV. The current cross-section is compared to the results of Mori *et al.*,[20] which shows a qualitative agreement throughout the entire energy range. However, below 10 eV, their results show a strange valley, which was absent in the previous cases. At high energies, their data slightly overestimate, probably due to the use of an independent atom model, which usually overestimates the cross section, in comparison with the single-centre approach of the present case. Overall, both results show qualitative agreement with each other.

Fig. 3b presents the total inelastic and its components (Q_{ps} and Q_{ion}) from about 10 eV to 5000 eV. The Q_{ps} with a magnitude of 0.07 Å^2 10 eV rises quickly to a maximum at 20 eV, measuring a cross section of 2.223 Å^2, before subsequently declining to zero at about 400 eV. The present Q_{ps} are shown along with the theoretical data of Mori *et al.*,[20] which is slightly higher in the energy range 8 eV to 30 eV, beyond which both values exhibit good alignment. The threshold of ionisation for HF is 16.03 eV; hence, this channel opens up after that. The

magnitude of Q_{ion} rises sharply once the channel is open and peaks at 70 eV with a maximum cross section of 1.639 Å^2, before reducing to 0.142 Å^2 at 5000 eV. The present Q_{ion} is compared with Mori *et al.*[20] as shown in the figure and is in excellent agreement. The total inelastic cross-section is also presented here along with Q_{ps}, Q_{ion}. It has a peak with a magnitude of 3.224 Å^2 at 35 eV and is subsequently reduced to 0.144 Å^2 at 5000 eV as expected.

The total elastic and inelastic cross sections for CF_4 are presented in Fig. 4. Fig. 4a shows the elastic and total cross sections from 1 eV to 5000 eV. The cross-section seems to follow a similar trend as that of HF. It increases gradually from 6.441 Å^2 to 9 Å^2 at about 9 eV, dips a bit and then exhibits a sudden increase upon the opening of inelastic channels, reaching its highest value of 20.764 Å^2 at 35 eV. Then it is followed by a slow decline to 1.133 Å^2 at 5000 eV. The present results are compared with the theoretical data reported by Mori *et al.*[20] and Baluja *et al.*[21] and the measurements of Sueoka *et al.*[24] The results of Mori *et al.*[20] show similar characteristics as observed in the case of F_2. Except around the peak, where our results are higher, the data shows reasonable agreement with the present one. The reasons for the deviations observed are as explained earlier. Furthermore, the tendency of our results to overestimate at lower energies is likely due to the overlap of charge densities, which are not accurately modelled. The values reported by Baluja *et al.*[21] are lower than the current data throughout the energy range, with their Q_{total} falling abruptly to match with the Q_{el}, which is not followed by other results. The present Q_{total} also exhibits reasonable agreement with the measurements presented by Sueoka *et al.*[24] These values also miss the hump near the maximum of positronium formation, which clearly indicates that they have not included this particular channel effectively. As we have reported earlier, at low energies, the experimental results lack forward angle correction, resulting in a discrepancy in the outputs.[51] The Q_{el} demonstrates a qualitative alignment with Mori *et al.*[20] over the entire energy spectrum, with minor variations.

The less pronounced hump in the case of Mori *et al.*[20] in Fig. 4a can be explained by the deviations observed in the comparison between the present Q_{ps} and theirs as shown in Fig. 4b. Even though at the beginning they go together from the threshold, the peak is slightly shifted and has a lower magnitude compared to our data. It clearly shows a rise, culminating at 20 eV, reaching a maximum value of 6.68 Å^2. Following this peak, a decline is observed, leading to a cross-section of zero above 200 eV. Present Q_{ps} is compared with the results of Mori *et al.*,[20] and both sets of results qualitatively demonstrate alignment across the full energy spectrum, with the current findings being shifted to higher energy and having a slower fall. After positronium formation, the ionisation channel opens, and the present Q_{ion} begins at 17 eV, rises to a maximum of 60 eV with a cross section of 7.997 Å^2, and then drops to 0.456 Å^2 at 50 eV. Both the present and Mori *et al.*'s[20] results demonstrate qualitative coherence. However, the current Q_{ion} peak is shifted towards lower energy and slightly higher value below 200 eV, and above that, it is lower and follows the present data. The Q_{inel} is also presented in the figure. Q_{inel} starts at 0.006 Å^2 at 9 eV, rises sharply, attaining a peak at 35 eV, which is apparently between the peaks of its components, Q_{ps} and Q_{ion} as expected. Thereafter, the inelastic cross section decreases and finally attains a value of 0.636 Å^2 merging with Q_{ion} at higher projectile energies. This is due to the fact that at those energies electrons interact with the target for a very short time, and thus the probability of excitation or ionisation decreases considerably.

Fig. 5a presents the elastic and total cross-section of C_2F_6, along with the available data.[20,25] The present total and elastic cross-sections follow a similar trend to that in Fig. 4a, but start a little lower, from 5.26 Å^2 at 1 eV. Q_{total} rises up to 6 eV and then again to 40.68 Å^2 at 25 eV as the inelastic channel contribution is added to the elastic. After this peak, it decreases to 1.902 Å^2 at 5000 eV. The present total cross section is compared with Mori *et al.*[20] and Sueoka *et al.*[25] Our results show a lower magnitude in the energy range 0–12 eV, and beyond that, a hump is observed,

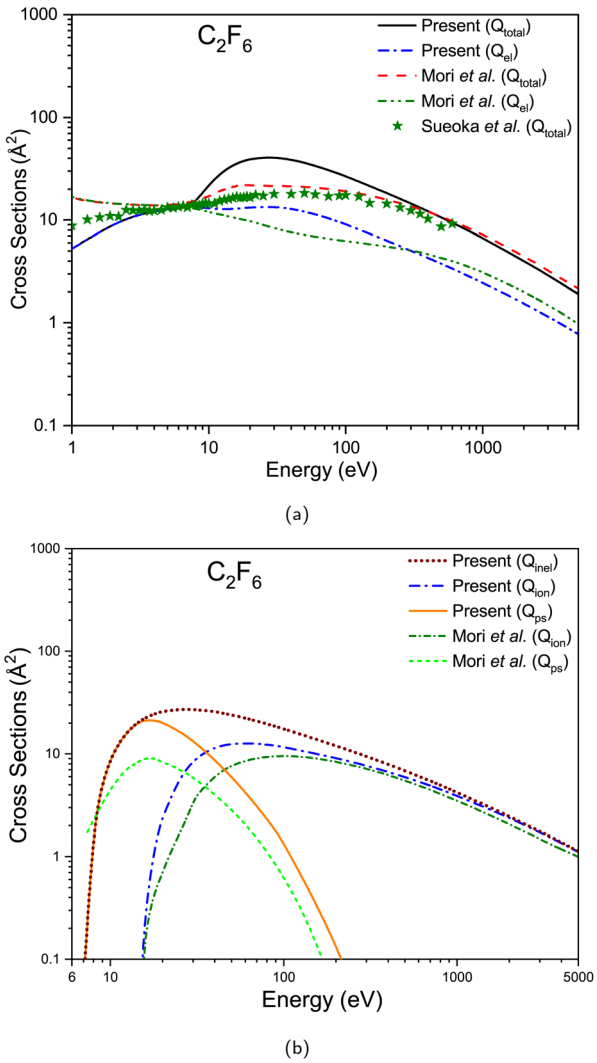

Fig. 5 Positron scattering from a C_2F_6 (a) Q_{total}: present – black solid, Mori *et al.* – red dash, Sueoka *et al.* – olive solid star; Q_{el}: present – blue dash dot, Mori *et al.* – olive dash dot dot. (b) Q_{inel}: present – wine short dot; Q_{ps}: present – orange solid, Mori *et al.* – green short dash; Q_{ion}: present – blue dash dot, Mori *et al.* – olive short dash dot.

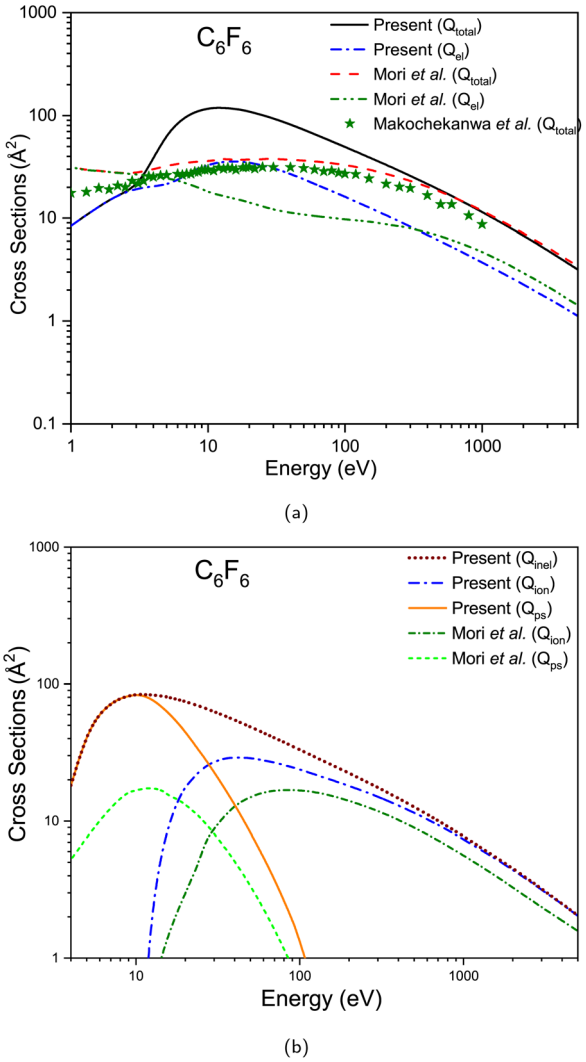

Fig. 6 Positron scattering from a C_6F_6 (a) Q_{total}: present – black solid, Mori *et al.* – red dash, Makochekanwa *et al.* – olive solid star; Q_{el}: present – blue dash dot, Mori *et al.* – olive dash dot dot. (b) Q_{inel}: present – wine short dot; Q_{ps}: present – orange solid, Mori *et al.* – green short dash; Q_{ion}: present – blue dash dot, Mori *et al.* – olive short dash dot.

which signifies the positronium formation channel. Above 200 eV, available experimental[25] and theoretical[20] results are in good agreement with the present results. The present Q_{el} decreases with increasing energy due to a limited effective interaction range similar to Mori *et al.*[20] except that the results of Mori *et al.*[20] fall off more rapidly in intermediate energy, indicating weaker elastic scattering and overestimating present data at high energy.

In Fig. 5b the present inelastic cross sections, *viz.*, positronium formation and ionisation, along with the available data[20] are plotted. The present Q_{ps} has similar characteristics to that of CF_4, with a maximum of 21.362 Å^2 at 17 eV, and falls to zero beyond 200 eV. Our result is higher than Mori *et al.*[20] in the entire energy range, as observed in the previous cases as well. Qualitatively, both cross sections follow a similar trend with a shifted peak. The ionisation cross section starts from 14 eV and peaks at 60 eV, where the cross section is 12.718 Å^2, before decreasing to 1.112 Å^2 at 5000 eV. Present Q_{ion} has a higher magnitude around the peak as compared with Mori *et al.*,[20] but is in good agreement with the increase in energy. The inelastic cross section begins at 7 eV with a value of 0.06 Å^2 and attains a maximum of 27.236 Å^2 at 25 eV. Subsequently, it decreases and attains a value of 1.126 Å^2 at 5000 eV. The inelastic results qualitatively correlate with the current findings of Q_{ion} and Q_{ps}.

C_6F_6 is like a benzene ring with hydrogen atoms replaced by fluorine. The electron impact scattering cross sections of C_6F_6 are presented in Fig. 6a and b. The elastic and total cross sections are shown in Fig. 6a. Besides the sharper lowering of the cross-section than in previous instances at the low energies, the overall shape looks similar. The Q_{total} peaks at 12 eV with a magnitude of 118.84 Å^2, while the elastic contribution is, in general, flat. Hence, this hump observed in the total is due to the inelastic channel, in particular the Q_{ps}, which is also evident from Fig. 6b. Our result is high in the intermediate energy as compared with the available experimental results of Makochekanwa *et al.*[19] and the theoretical results of Mori *et al.*[20] The present cross-section is low below 8 eV, and above that, it is overestimated. One of the reasons may be due to the fact that the present cross-section is calculated by the simple additivity rule. At higher energies, above 200 eV, the present and available cross sections start aligning well. The current elastic cross-section has a lower cross-section below 8 eV and a higher cross-section above that in comparison with Mori *et al.*[20] till around 300 eV. Beyond that, both results agree with each other well.

Positronium formation in C_6F_6 is quite large and contributes most of the inelastic cross section below 10 eV, as shown in Fig. 6b, while the ionisation starts above that energy. The available data of Mori *et al.*[20] is quite low for both cases, especially around the peak. Q_{pos} has a maxima at 10 eV, similar to the available data, but with higher magnitude. It decreases steeply beyond that and becomes zero above 400 eV. The peak of the present Q_{ion} is shifted to the lower energy side than that of Mori *et al.*[20] This large discrepancy needs further attention, and more theoretical and experimental studies are required for cyclic molecules. We have also reported the inelastic cross sections here. Prior to the ionisation threshold, positronium formation contributes mostly to it. Then ionisation takes over and becomes the majority contributor at high energies. For the C_6F_6 molecule, which is cyclic in nature, all cross sections presented are high, and this may be because of the cyclic nature, which has delocalized π-electron density, which needs to be considered properly in the calculation for better results.

In Fig. 7, the total elastic and inelastic cross-sections for CHF_3 are presented, in which one fluorine atom of CF_4 is replaced by a hydrogen atom, which makes it more suitable for applications requiring higher etching selectivity. In comparison to CF_4 scattering cross-sections, those of CHF_3 show a similar trend. Its total cross-section is obtained by adding CH the group, with thrice of fluorine atom cross section, and taking into account the molecular properties of CHF_3. The total cross-section is presented in Fig. 7a. The present Q_{total} is 4.83 Å^2 at

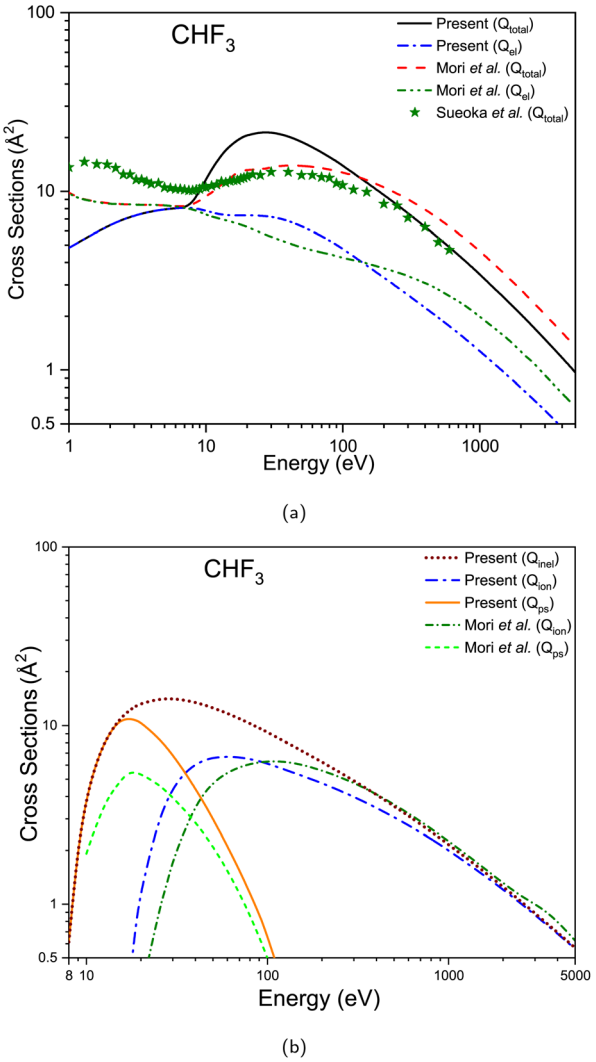

Fig. 7 Positron scattering from a CHF_3 (a) Q_{total}: present – black solid, Mori *et al.* – red dash, Sueoka *et al.* – olive solid star; Q_{el}: present – blue dash dot, Mori *et al.* – olive dash dot dot. (b) Q_{inel}: present – wine short dot; Q_{ps}: present – orange solid, Mori *et al.* – green short dash; Q_{ion}: present – blue dash dot, Mori *et al.* – olive short dash dot.

1 eV, which is lower than the available result[20,23] and further total cross section increases with energy. At 10 eV, the present and available theoretical data of Mori *et al.*[20] coincide, while the experimental[23] cross section is overestimated. After 10 eV, there is a sudden increase of total cross section to 21.422 Å^2 at 25 eV, and a similar trend is followed by available results.[20,23] Subsequently, the cross-section decreases gradually with energy and reaches 0.968 Å^2 at 5000 eV, an obvious response similar to CF_4. For the intermediate energy range, the hump in the present result is higher than both available results,[20,23] for similar reasons as CF_4. The elastic cross-section of Mori *et al.*[20] is showing a dip in the intermediate energy and overestimates the present cross-section in low energy and in high energy. While the present Q_{el} smoothly starts and attains a peak at 10 eV, and afterwards the magnitude decreases as the elastic interaction reduces with the higher velocity of the projectile. Qualitatively, the shape of both cross sections aligns well, with some difference in magnitude.

The positronium formation cross-section of CHF_3 shows interesting characteristics, as both Mori *et al.*[20] and the present have lower magnitudes with similar characteristics as CF_4. The shift of the peak of Q_{pos} of CHF_3 towards higher energy and a similar trend for the shift of the peak towards lower energy for Q_{ion} is seen that shows correlation among them and also methodological difference to extract Q_{pos} and Q_{ion} from total inelastic cross sections, all of these presented in Fig. 7b. Positronium formation is showing good agreement with Mori *et al.*[20] qualitatively. The present Q_{pos} of 0.344 Å^2 at 10 eV increases to maximum 6.68 Å^2 at 20 eV. The magnitude of Mori's positronium formation cross-section is lower than the present result. The ionisation cross-section of Mori *et al.*[20] shows a shifted peak towards higher energy. The magnitude of the present Q_{ion} is higher than the available result[20] up to 200 eV; thereafter, the present result underestimates. Additionally, the total inelastic cross-section of CHF_3 is presented, which increases from 9 eV onwards, and the magnitude of the cross-section at the peak is 13.277 Å^2 at 35 eV; simultaneously with an increase in energy, the cross-section decreases to 0.636 Å^2 at 5000 eV, which is quite obviously due to low interaction because of the high speed of the projectile.

In Fig. 8, fluorine-substituted alkene $C_2H_2F_2$ cross-sections are reported. In Fig. 8a we present the total cross section, which shows a hump in intermediate energy, definitely due to the inclusion of positronium formation, which seems to be absent in available experimental[26] results. Present Q_{total}, slightly lower value than experimental,[26] increases with energy, and at 14 eV it attains a maximum of 40.193 Å^2. Available data[26] is almost constant till 100 eV, which shows the absence of positronium formation. It starts decreasing after 100 eV, and from 200 eV onwards, the present result is in excellent agreement with the measurements of Makochekanwa *et al.*[26] The Q_{el} is presented along with the theoretical result of Baluja *et al.*[22] Present Q_{el} and available data of Baluja *et al.*[22] shows excellent agreement for energy above 20 eV. Also, at 20 eV, the experimental Q_{total} is close to the elastic results, which is not expected. Further present Q_{el} increases from 1 eV, where the cross section is 6.256 Å^2, and peaks at 16 eV, and decreases to 0.399 Å^2 at 5000 eV. Present results, from 1 to 10 eV, are lower than the available cross-section.[22] Qualitatively, both the present and Baluja *et al.*[22] elastic cross-sections are in reasonable agreement for the high energy range.

For $C_2H_2F_2$, Q_{inel}, Q_{ion} and Q_{pos} are presented in Fig. 8b along with the theoretical Q_{ion} of Baluja *et al.*[22] The Q_{pos} becomes maximum at 11 eV; till then, it is purely contributing to Q_{inel}. The ionisation channel opens after the threshold and contributes to the total inelastic cross-section, and at high energy, Q_{ion} and Q_{inel} seem to overlap. Present Q_{ion} starts with a magnitude of 0.02 Å^2 at 11 eV, and with an increment in energy, ionisation increases, and it peaks at 45 eV, where the cross-section is 10.549 Å^2. Subsequently, it reduced to 0.686 Å^2 at 5000 eV. The present Q_{ion} results are in agreement with the available data.[22] For the energy range of 20 to 100 eV, the present result is high. This discrepancy is due to the theoretical models used to obtain

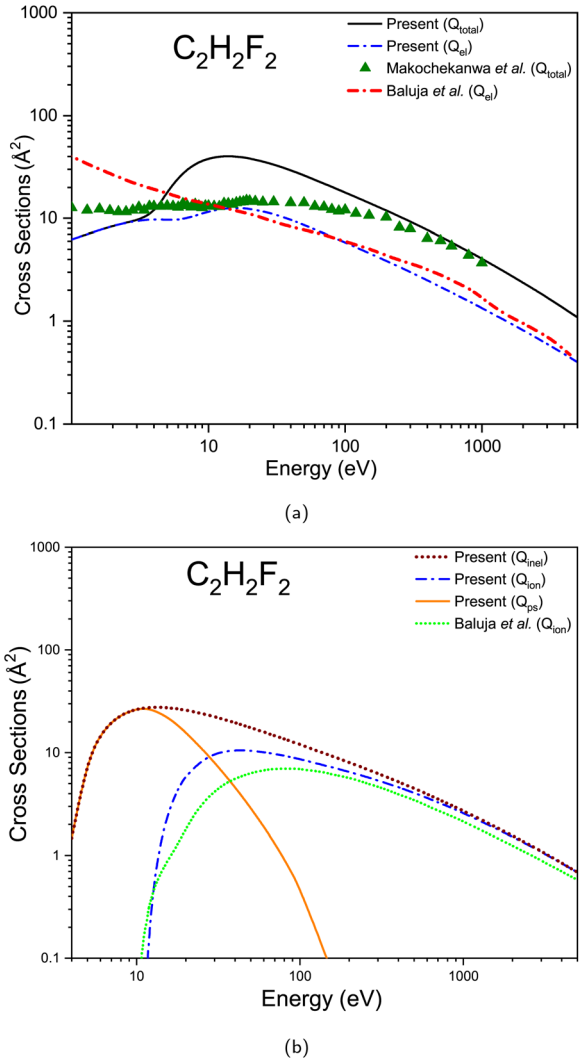

Fig. 8 Positron scattering from a $C_2H_2F_2$ (a) Q_{total}: present – black solid, Makochekanwa *et al.* – olive solid star; Q_{el}: present – blue dash dot, Baluja *et al.* – red short dash dot, (b) Q_{inel}: present – wine short dot; Q_{ps}: present – orange solid; Q_{ion}: present – blue dash dot, Baluja *et al.* – olive short dash dot.

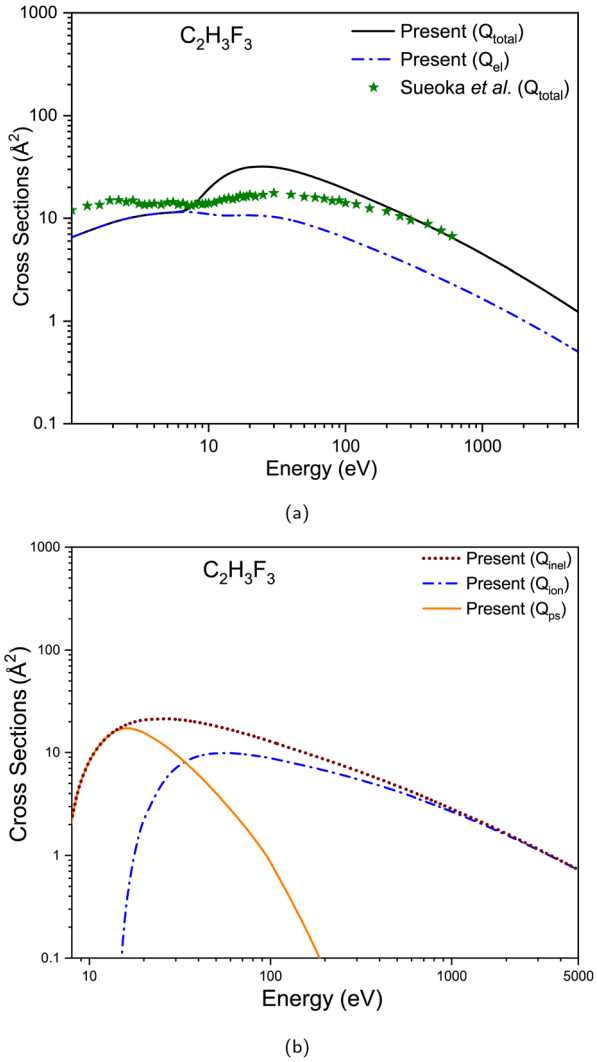

Fig. 9 Positron scattering from a $C_2H_3F_3$ (a) Q_{total}: present – black solid, Sueoka *et al.* – olive solid star; Q_{el}: present – blue dash dot. (b) Q_{inel}: present – wine short dot; Q_{ps}: present – orange solid; Q_{ion}: present – blue dash dot.

Q_{ion}; hence, further study is required to verify this. The inelastic cross section is presented and shows good correlation with its constituents. It starts from 4 eV with a magnitude of 1.457 Å^2, and attains its peak at 13 eV, where Q_{ion} and Q_{pos} contributions are maximum, and after that, it gradually decreases with energy.

In Fig. 9, the cross-section of $C_2H_3F_3$ is presented, in which three fluorine atoms are replaced by hydrogen as compared to C_2F_6, this will reduce the magnitude of the cross-section of $C_2H_3F_3$ but expected to have a similar trend. Fig. 9a presents the total cross-section starting from 1 eV, which increases gradually till 10 eV, where present and experimental[25] data coincide. The experimental result is higher than the present with a dip at 10 eV and then increases similarly to the present results. Our result has a hump at around 25 eV, where the cross-section is 32.066 Å^2. Q_{total} shows a decreasing trend with energy; as the cross-section decreases, it falls to 1.23 Å^2 at 5000 eV. Above 200 eV, the present cross-section and Sueoka *et al.*'s.[25] experimental results agree with each other. The discrepancy in the energy range 10 eV to 200 eV is due to the overlapping charge density, as explained earlier. Along with the Q_{total}, we presented the Q_{el}, which contributes to the total cross-section completely till 7 eV, and afterwards it starts decreasing and reaches a minimum of 0.504 Å^2 at 5000 eV. There is no available data for comparison, but it shows a similar trend as C_2F_6 with a lower magnitude.

There is no data available for the inelastic cross sections of $C_2H_3F_3$ as evident from Fig. 9b. It is very clear from the figure that Q_{ps} contributes mostly at low energies and Q_{ion} at high energies. This is expected, as evident from our previous results. Presents Q_{ps}, which opens at 7 eV and rises with energy and peaks at 16 eV with magnitude 17.268 Å^2, then it shows a downward trend and becomes zero above 500 eV. The ionisation channel opens at 13 eV, and the cross-section rises to

9.903 Å^2 at 60 eV, where ionisation is maximum. Beyond this point, it gradually decreases to a value of 0.719 at 5000 eV. The total inelastic cross section starts from 0.39 Å^2 at 7 eV, increases initially by the contribution of Q_{ps}, and then due to ionisation channel above ionisation threshold. The Q_{inel} attains maximum of 21.467 Å^2 at 25 eV, afterwords it reduces to 0.726 Å^2 at 5000 eV as interaction time decreases at higher energies. This is a similar trend we observed in all the above studies, and to verify the results, we need further theoretical and experimental investigations.

3.2 Comparative study of total and ionization cross section

Fig. 10 is a comparative study of all the target molecules in the present work, and it is quite evident that the cross-section is highly dependent on the number of electrons, bond order, and the molecular properties. In Fig. 10a, the total cross sections are presented, and the cross section of HF below 5 eV is higher than that of F_2. This may be due to the use of single-center expansion for HF and the modified additivity rule for F_2. Further, in the case of $C_2H_2F_2$ and C_6F_6, the hump in the total cross section appears at a lower energy than other targets as the ionisation potential of these molecules are lowest. The total cross section increases with the number of electrons at higher energies for all molecules, but at lower energies, it differs. This variation is due to the difference in molecular properties such as polarizability, dipole moment, and ionisation potential, which affects the cross section significantly at low energies. Fig. 10b presents the ionisation cross-section, which increases with the number of electrons. Ionisation potential decreases in the order of F > HF > F_2 > CF_4 > CHF_3 > C_2F_6 > $C_2H_2F_2$ > C_6F_6, and hence the peak of the ionisation cross section shifts to lower energies. Beyond the peak, the cross-section of all targets decreases gradually with the increase in energy monotonously.

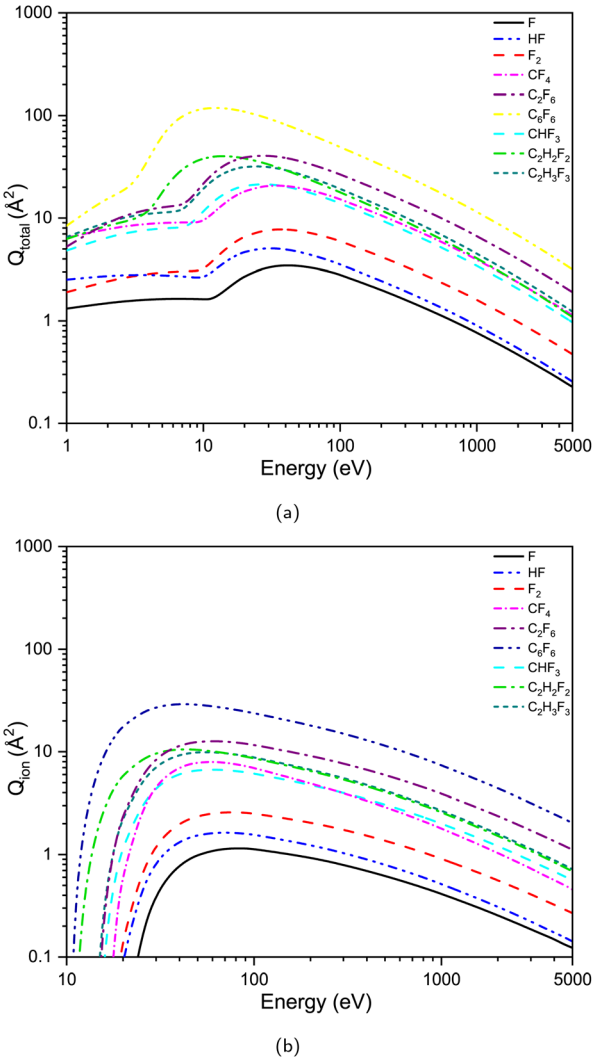

Fig. 10 Positron scattering cross-section (a) Q_{total} and (b) Q_{ion}: F – solid (Black), F_2 – dash (Red), HF – dash dot dot (Blue), CF_4 – short dash dot (Magenta), CHF_3 – dash (Cyan), C_6F_6 – dash dot dot (Royal Blue), $C_2H_3F_3$ – short dash (Dark Cyan), $C_2H_2F_2$ – dash dot (Parrot Green), C_2F_6 – dash dot (Purple).

4 Conclusions

The positron scattering cross-sections, elastic, inelastic, total, ionisation, and positronium formation, for a range of fluorine-containing molecules using the SCOP and CSP-ic methods are presented here. For the fluorine atom, the present and available cross sections of Mori *et al.*[20] are in good agreement except below the positronium formation threshold, where the present cross section is high. Similarly, for the F_2 and HF molecules, both present and Mori *et al.*[20] give consistent positron scattering cross-sections. For other target molecules, the present cross-section at intermediate energies (10–200 eV) is high, which may be due to the overlapping of charge densities. However, at high energies above 200 eV, total cross sections are in close agreement with the experimental results. However, further investigation is required for hydrofluorocarbons, which is a first-time study.

The cross-section presented in this study plays a significant role in understanding how positrons lose energy, create ions, and form positronium. In radiation physics, positron interactions have applications in PET scans, wherein positronium is formed and subsequently annihilates into two gamma rays, which are utilized for imaging purposes. Fluorine is highly electronegative, creating strong polar bonds and dense localised electron clouds. The positron, being sensitive to these electron densities, acts as a probe to map the electronic structure, and so it is used in material science. Additionally, the HF molecule is present in interstellar clouds, and the cross-sections presented in this study are useful for astrochemists for modelling positron collision processes in space.

Author contributions

Ashutosh Yadav: conceptualisation; data curation; formal analysis; investigation; methodology; software; writing – original draft. Bobby Antony: conceptualisation; resources; supervision; methodology; validation; writing – review & editing.

Conflicts of interest

There are no conflicts to declare.

Data availability

The data supporting this article have been included as part of the supplementary information (SI). Supplementary information: numerical cross-section data for present targets (PDF). See DOI: https://doi.org/10.1039/d6ra01378c.

Acknowledgements

The author gratefully acknowledges Dr Nicolas A. Mori (University of Cambridge) for kindly providing the positron scattering cross-section data used in this work.

References

1 C. Makochekanwa, O. Sueoka and M. Kimura, *J. Phys.: Conf. Ser.*, 2007, **80**, 012012.
2 T. Nishimura and F. Gianturco, *J. Phys. B: At. Mol. Opt. Phys.*, 2003, **37**, 215.
3 F. Selim, *Mater. Charact.*, 2021, **174**, 110952.
4 I. Chakraborty, N. Uddin and B. Antony, *RSC Adv.*, 2024, **14**, 38855–38863.
5 A. Ghoshal, M. Kamali and K. Ratnavelu, *Phys. Plasmas*, 2013, **20**, 013506.
6 T. Siegert, R. Crocker, R. Diehl, M. Krause, F. Panther, M. Pleintinger and C. Weinberger, *Astron. Astrophys.*, 2019, **627**, A126.
7 T. C. Naginey, B. B. Pollock, E. W. Stacy, H. R. J. Walters and C. T. Whelan, *Phys. Rev. A*, 2014, **89**, 012708.
8 M. E. Phelps, *Proc. Natl. Acad. Sci. U. S. A.*, 2000, **97**, 9226–9233.
9 S. Jan, G. Santin, D. Strul, S. Staelens, K. Assié, D. Autret, S. Avner, R. Barbier, M. Bardiès, P. Bloomfield, D. Brasse, V. Breton, P. Bruyndonckx, I. Buvat, A. Chatziioannou, Y. Choi, Y. Chung, C. Comtat, D. Donnarieix and C. Morel, *Phys. Med. Biol.*, 2004, **49**, 4543–4561.
10 S. Mahla and B. Antony, *RSC Adv.*, 2024, **14**, 1397–1406.
11 C. M. Surko, A. Passner, M. Leventhal and F. J. Wysocki, *Phys. Rev. Lett.*, 1988, **61**, 1831–1834.
12 J. R. Danielson, D. H. E. Dubin, R. G. Greaves and C. M. Surko, *Rev. Mod. Phys.*, 2015, **87**, 247–306.
13 M. Zammit, D. Fursa and I. Bray, *Phys. Rev. A*, 2013, **87**, 020701.
14 L. Dalagnol, G. Moreira, A. Souza Barbosa and M. Bettega, *J. Phys. Chem. A*, 2023, **127**, 6486–6494.
15 S. Falcinelli, F. Vecchiocattivi, B. G. Brunetti, M. Parriani, G. Gigliotti, S. Stranges and F. Pirani, *RSC Adv.*, 2022, **12**, 7587–7593.
16 S. Singh and B. Antony, *Phys. Plasmas*, 2018, **25**, 053503.
17 D. Gupta, H. Choi, M.-Y. Song, G. Karwasz and J.-S. Yoon, *Eur. Phys. J. D*, 2017, **71**, 88.
18 G. Karwasz, P. Mozejko and M.-Y. Song, *Int. J. Mass Spectrom.*, 2014, **365–366**, 232–237.
19 C. Makochekanwa, O. Sueoka and M. Kimura, *Phys. Rev. A*, 2003, **68**, 032707.
20 N. Mori, H. Umer, L. Scarlett, I. Bray and D. Fursa, *J. Phys. B: At. Mol. Opt. Phys.*, 2024, **57**, 225201.
21 K. L. Baluja and A. Jain, *Phys. Rev. A*, 1992, **45**, 7838–7845.
22 A. Arora, V. Sahgal, A. Bharadvaja and K. Baluja, *Phys. Rev. A*, 2021, **104**, 022816.
23 O. Sueoka, H. Takaki, A. Hamada, H. Sato and M. Kimura, *Chem. Phys. Lett.*, 1998, **288**, 124–130.
24 O. Sueoka, S. Mori and A. Hamada, *J. Phys. B: At. Mol. Opt. Phys.*, 1994, **27**, 1453.
25 O. Sueoka, C. Makochekanwa and H. Kawate, *Nucl. Instrum. Methods Phys. Res., Sect. B*, 2002, **192**, 206–214.
26 C. Makochekanwa, H. Kato, M. Hoshino, M. H. F. Bettega, M. A. P. Lima, O. Sueoka and H. Tanaka, *J. Chem. Phys.*, 2007, **126**, 164309.
27 Ü. Kavak, F. F. S. van der Tak, A. G. G. M. Tielens and R. F. Shipman, *Astron. Astrophys.*, 2019, **631**, A117.
28 D. G. Cocks, H. Chaudhary and J. R. Machacek, *Acta Pathol. Jpn.*, 2019, **878**, 123.
29 S. Marjanovic, A. Banković, D. Cassidy, B. Cooper, A. Deller, S. Dujko and Z. Petrović, *J. Phys. B: At. Mol. Opt. Phys.*, 2016, **49**, 215001.
30 C. Baker, C. Isaac, D. Edwards, H. Evans, R. Clayton, D. van der Werf and M. Charlton, *J. Phys. B: At. Mol. Opt. Phys.*, 2020, **53**, 185201.
31 R. Dussart, R. Ettouri, J. Nos, G. Antoun, T. Tillocher and P. Lefaucheux, *J. Appl. Phys.*, 2023, **133**, 113306.
32 N. Lim, A. Efremov and K.-H. Kwon, *Plasma Chem. Plasma Process.*, 2021, **41**, 1671–1689.
33 A. Anus, M. Sheraz, S. Jeong, E. kun Kim and S. Kim, *J. Anal. Appl. Pyrolysis*, 2021, **156**, 105126.
34 D. Toneli, R. Pessoa, M. Roberto and J. Gudmundsson, *Plasma Sources Sci. Technol.*, 2019, **28**, 025007.
35 B. Goswami and B. Antony, *RSC Adv.*, 2014, **4**, 30953–30962.
36 D. Gupta, R. Naghma, B. Goswami and B. Antony, *RSC Adv.*, 2014, **4**, 9197–9204.
37 B. Goswami, R. Naghma and B. Antony, *RSC Adv.*, 2014, **4**, 63817–63823.
38 J. Kaur, R. Naghma and B. Antony, *RSC Adv.*, 2015, **5**, 20090–20097.
39 S. Mahla and B. Antony, *J. Appl. Phys.*, 2023, **134**, 124901.
40 H. Cox Jr and R. Bonham, *J. Chem. Phys.*, 1967, **47**, 2599–2608.
41 X. Zhang, J. Sun and Y. Liu, *J. Phys. B Atom. Mol. Opt. Phys.*, 1992, **25**, 1893.
42 J. Perdew and A. Zunger, *Phys. Rev. B*, 1981, **23**, 5048–5079.
43 D. Reid and J. Wadehra, *J. Phys. B: At. Mol. Opt. Phys.*, 1996, **29**, L127.
44 L. Chiari, A. Zecca, S. Girardi, E. Trainotti, G. García, F. Blanco, R. P. McEachran and M. J. Brunger, *J. Phys. B: At. Mol. Opt. Phys.*, 2012, **45**, 215206.
45 A. Yadav and B. Antony, *J. Phys. Chem. A*, 2025, **129**, 8013–8023.
46 S. Singh, S. Dutta, R. Naghma and B. Antony, *J. Phys. B: At. Mol. Opt. Phys.*, 2017, **50**, 135202.

47 R. Naghma, D. Gupta, B. Goswami and B. Antony, *Int. J. Mass Spectrom.*, 2014, **360**, 39–44.
48 H. Deutsch, K. Becker, S. Matt and T. Märk, *Int. J. Mass Spectrom.*, 2000, **197**, 37–69.
49 R. Naghma and B. Antony, *J. Electron Spectrosc. Relat. Phenom.*, 2013, **189**, 17–22.
50 CCCBDB, Computational chemistry comparison and benchmark database, https://cccbdb.nist.gov/, accessed 20-April-2025.
51 M. J. Brunger, S. J. Buckman and K. Ratnavelu, *J. Phys. Chem. Ref. Data*, 2017, **46**, 023102.